No. 1C-a16 $KNbO_3$–$KTaO_3$ (including KTN)

1b	Phase diagram: Figs. 1C-a16-001...1C-a16-003. The crystal of $K(Ta_{1-x}Nb_x)O_3$ with x between about 0.35 and 0.45 is called KTN.	
3b	Structural parameters: Table 1C-a16-001.	
5a	Dielectric constant: Figs. 1C-a16-004...Fig. 1C-a16-009.	
c	Spontaneous polarization and pyroelectricity: Fig. 1C-a16-010.	
6a	Specific heat: Fig. 1C-a16-011, Fig. 1C-a16-012; Table 1C-a16-002.	
7a	Piezoelectricity: Fig. 1C-a16-013.	
b	Electrostriction: Fig. 1C-a16-014.	
8a	Elastic compliance: Fig. 1C-a16-015; see also Effect of biasing electric field on elastic stiffness: see	81Law 90Tou
9a	Refractive index: Fig. 1C-a16-016. Absorption: Fig. 1C-a16-017; see also Infrared reflection: Fig. 1C-a16-018.	 86Tsu
b	Electrooptic effect: Fig. 1C-a16-019. Quadratic electrooptic effect: see Electroreflectance: see	 71Fox 67Fro
d	Faraday effect: Fig. 1C-a16-020.	
10a	Raman scattering: Table 1C-a16-003, Fig. 1C-a16-021, Fig. 1C-a16-022; see also	84Kug
b	Brillouin scattering: see	85Lee
13a	NMR: Fig. 1C-a16-023.	
b	ESR: Fig. 1C-a16-024.	
14b	Phonon dispersion: Fig. 1C-a16-025, Fig. 1C-a16-026. Soft mode intensity: Fig. 1C-a16-027. Neutron scattering intensity: Fig. 1C-a16-028.	
15a	Domain observation by transmission electron microscope: see	93XuH
16	Photorefractive effect: see Thin film: see	80Boa 92Gut, 94Ger

Table 1C-a16-001. $K(Ta_{0.56}Nb_{0.44})O_3$. Structural parameters [72Hew].

Δz(K)	0.012(4) *a*	U_{11}(O(1)) = U_{22}(O(1))	0.007(1) [Å^2]
Δz(Ta, Nb)	0.0 (origin)	U_{33}(O(1))	0.0042(7) [Å^2]
Δz(O(1))	–0.0101(8) *a*	U_{11}(O(2)) = U_{22}(O(3))	0.008(1) [Å^2]
Δz(O(2)) = Δz(O(3))	–0.0115(8) *a*	U_{22}(O(2)) = U_{11}(O(3))	0.0050(3) [Å^2]
U_{11}(K) = U_{22}(K)	0.004(2) [Å^2]	U_{33}(O(2)) = U_{33}(O(3))	0.0073(7) [Å^2]
U_{33}(K)	0.009(1) [Å^2]	ε	0.00097(7)
U_{11}(Ta, Nb) = U_{22}(Ta, Nb)	0.005(1) [Å^2]	*R*	0.021
U_{33}(Ta, Nb)	0.009(1) [Å^2]	R_w	0.025

Δz: Displacement along [001] from the atomic positions for cubic perovskite (in fractional coordinate change with a = 4.006 Å). $U_{jj} = \langle u_j \rangle^2$: Mean square amplitude of vibration along j-axis.
ε: Extinction parameter; R: Reliability index (R_w: weighted R).

Table 1C-a16-002. $K(Nb_{1-x}Ta_x)O_3$. Thermal parameters [59Hal]. L: latent heat, Θ_f: Curie temperature, A: a constant in the formula of free energy density $F = (A/\varepsilon_0)(T - \Theta_p)P^2 + ...$

x	L [J mol^{-1}]	Θ_f [K]	A [$\cdot 10^5$ K^{-1}]
0	460(42)	679	2.6
0.06	190(17)	656	2.7
0.12	42(8)	623	2.85
0.18	17(8)	591	3.05

Table 1C-a16-003. $K(Ta_{0.64}Nb_{0.36})O_3$. Raman frequencies $\Delta\nu$ and assignments at T = – 20°C. [a]) [72Man1], [b]) [68Fle], [c]) [66Bar]. Overtones and combination of two-phonon bands are indicated by notation as $2TO_4$ and $TO_4 + TO_2$, respectively. Frequencies assigned in brackets are not observed, but expected from comparison with the results for other perovskite-type compounds. The assignments indicated in curly braces are only speculative. Lines at 13.1 and $5.25\cdot10^{12}$ Hz may be due to zero-boundary phonons. The line at $24.8\cdot10^{12}$ Hz shows well-defined degenerated character of $A_1(TO)$ + E(TO) + F, where F represents a forbidden symmetry structure observed in $X(YX)X$ spectrum.

$\Delta\nu$ [$\cdot10^{12}$ Hz]							
First order [a])		Second order [a])		First order induced Raman [b])		IR [c])	
		51.6	$2LO_4$				
		31.2	$2TO_4$				
		26.1	$2LO_2$				
24.8	$A_1(TO)+E(TO)+F+[LO_4]$					25.0	LO_4
		22.5	TO_4+TO_2				
		20.7	TO_4+TO_1				
		16.8	TO_4+TA				
16.7	$A_1(TO_4)+E(TO_4)$			16.7	$A_1(TO_4)$	16.5	TO_4
		13.9	TO_4–TA				
13.1	{ZB LO_2}						
12.6	$E(LO_2)$					12.7	LO_2
8.37	$E(TO_3)+F+[E(LO_3)]$						
8.25	B_1						
6.06	$A_1(TO_2)+E(TO_2)+F+[LO_1]$			5.94	$A_1(TO_2)$	5.97	TO_2
						5.64... 5.88	LO_1
5.25	{ZB TO_1}						
4.20	$A_1(TO)$						
3.90	E(TO)						
		3.60	2TA				
2.55	$A_1(TO_1)$			2.55	$A_1(TO_1)$	2.55	TO_1
1.05	$E(TO_1)$ wing						

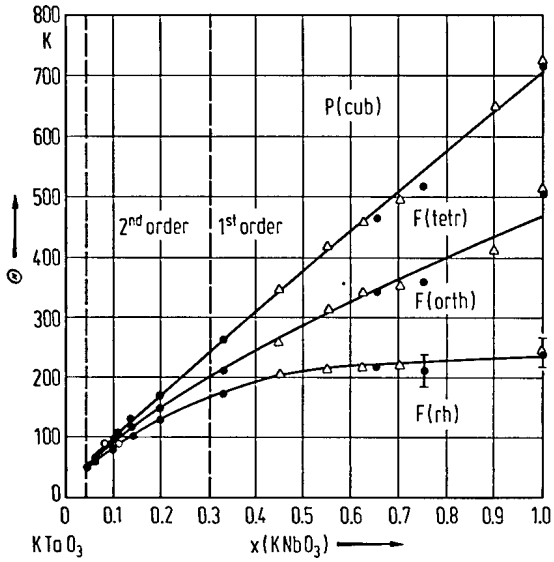

Fig. 1C-a16-001. $K(Ta_{1-x}Nb_x)O_3$. Θ vs. x. Triangles: [59Tri], open circles: [70Tod], full circles: [76Per].

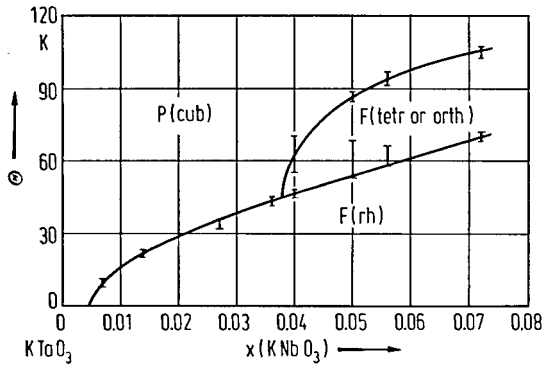

Fig. 1C-a16-002. $K(Ta_{1-x}Nb_x)O_3$. Θ vs. x [77Boa]. Determined from the measurements of P_s by low frequency hysteresis loop method and the temperature dependence of κ. See also [77Hoc].

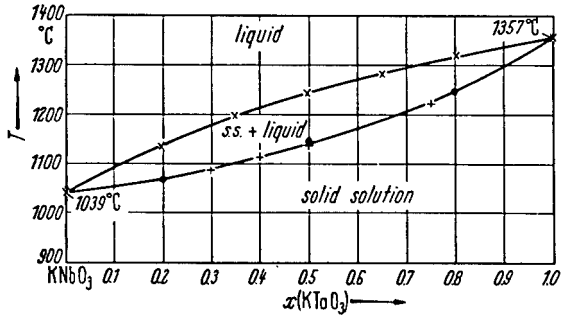

Fig. 1C-a16-003. $K(Nb_{1-x}Ta_x)O_3$. Phase diagram [55Rei]. Method: crosses: cooling curves, plus signs: conductivity curves, full circles: heating curves.

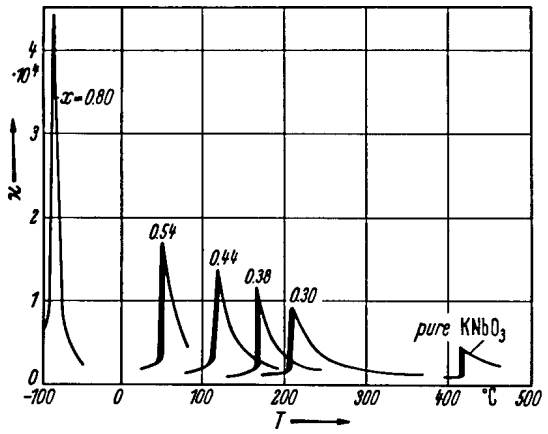

Fig. 1C-a16-004. $K(Nb_{1-x}Ta_x)O_3$. κ vs. T [59Tri]. Parameter: x. f = 10 kHz.

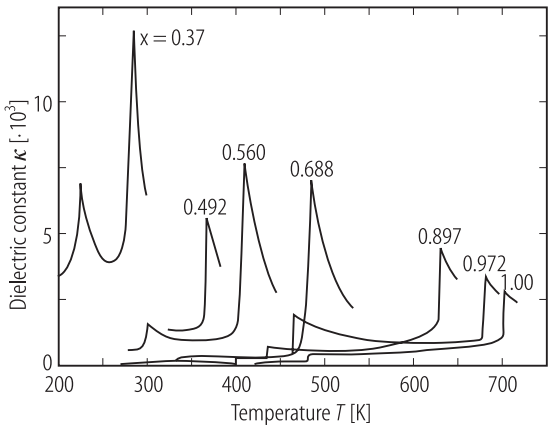

Fig. 1C-a16-005. $K(Ta_{1-x}Nb_x)O_3$. κ vs. T [89Bal]. Parameter: x. f = 100 kHz.

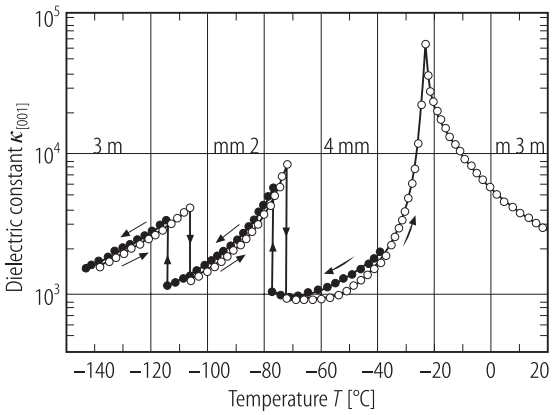

Fig. 1C-a16-006. $K(Ta_{0.68}Nb_{0.32})O_3$: Cu. $\kappa_{[001]}$ vs. T [92Wan]. f = 1 kHz. Crystal was poled along [001].

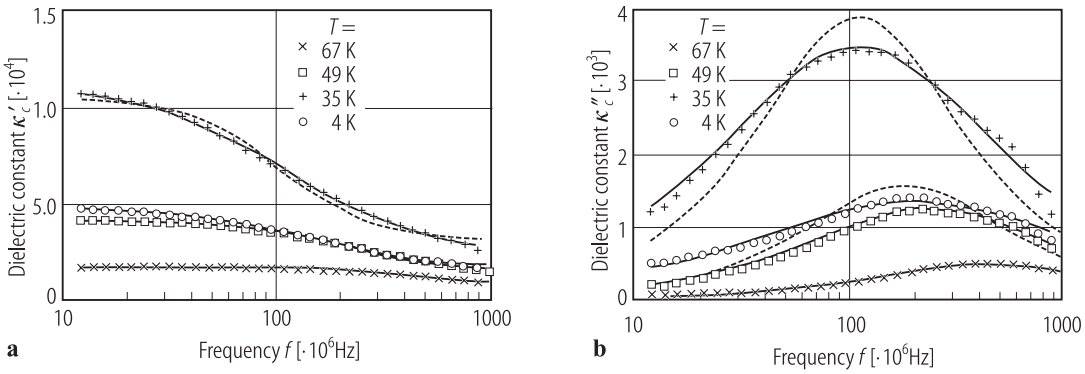

Fig. 1C-a16-007. $K(Ta_{0.96}Nb_{0.04})O_3$. κ_c', κ_c'' vs. f [93Fon]. Parameter: T. Broken lines: Debye formula $\kappa_c - \kappa_\infty = \Delta\kappa / (1 + i\,\omega\,\tau)$, where $\kappa_c = \kappa_c' - i\kappa_c''$ and κ_∞, $\Delta\kappa$, τ are constants independent of f. Full lines: Debye-Wagner formula $\kappa_c - \kappa_\infty = \Delta\kappa \int g(\tau)\, d\tau / (1 + i\,\omega\,\tau)$, where $g(\tau)$ is a log-normal distribution function of τ.

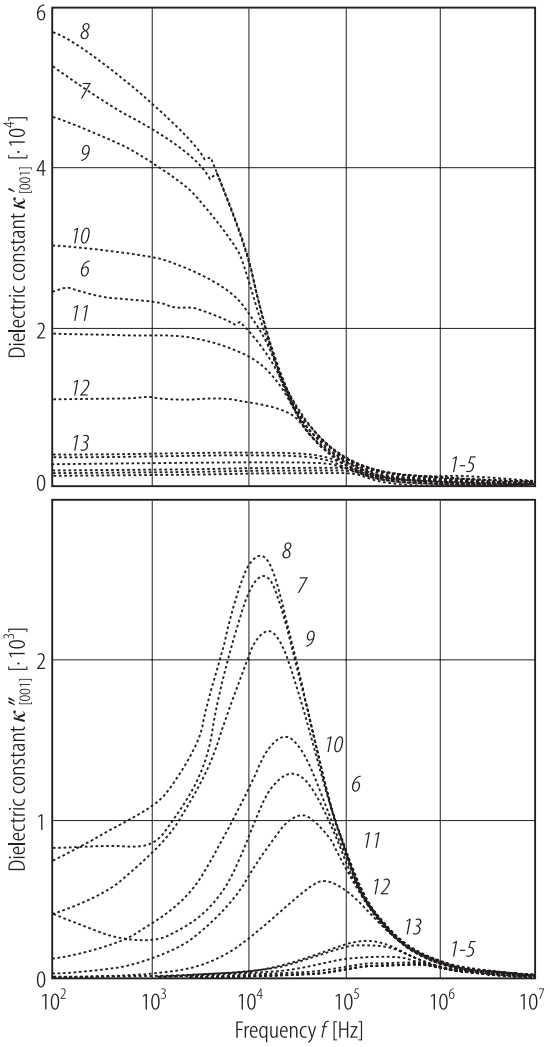

Fig. 1C-a16-008. $K(Ta_{0.97}Nb_{0.03})O_3$. $\kappa'_{[001]}$, $\kappa''_{[001]}$ vs. f [91Som]. Parameter: T. Curve *1*: T = 7.2 K, *2*: 11.1 K, *3*: 17.7 K, *4*: 24.2 K, *5*: 30.6 K, *6*: 38.9 K, *7*: 41.5 K, *8*: 43.4 K, *9*: 45.3 K, *10*: 47.1 K, *11*: 48.9 K, *12*: 51.7 K, *13*: 60.9 K.

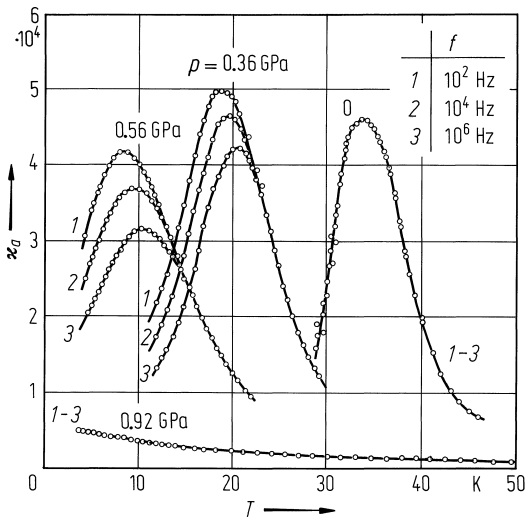

Fig. 1C-a16-009. $K(Ta_{0.98}Nb_{0.02})O_3$. κ_a vs. T [84Sam]. Parameter: p, f.

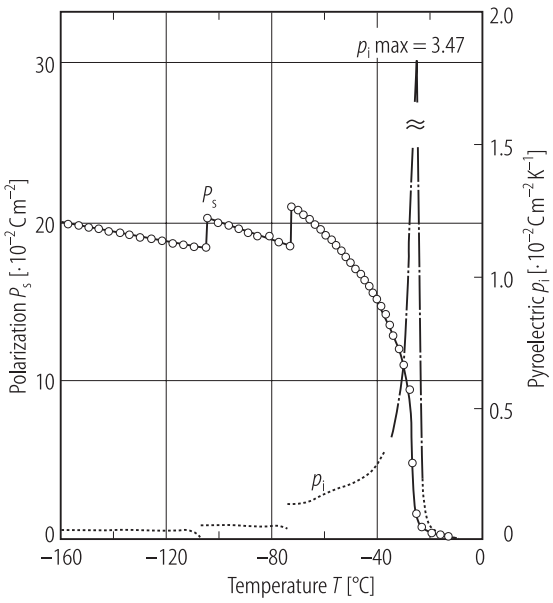

Fig. 1C-a16-010. $K(Ta_{0.68}Nb_{0.32})O_3$: Cu. P_s, p_i vs. T [92Wan]. p_i: pyroelectric coefficient.

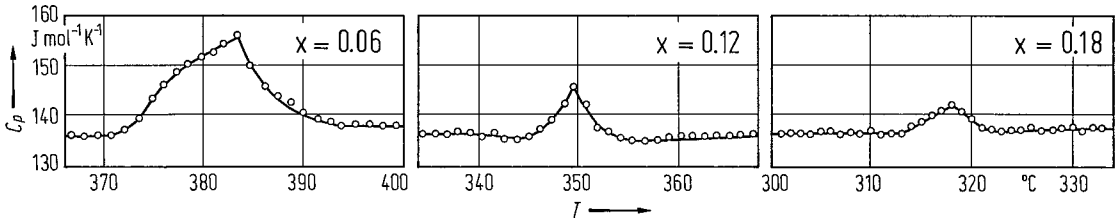

Fig. 1C-a16-011. $K(Nb_{1-x}Ta_x)O_3$. C_p vs. T [59Hal]. Parameter: x.

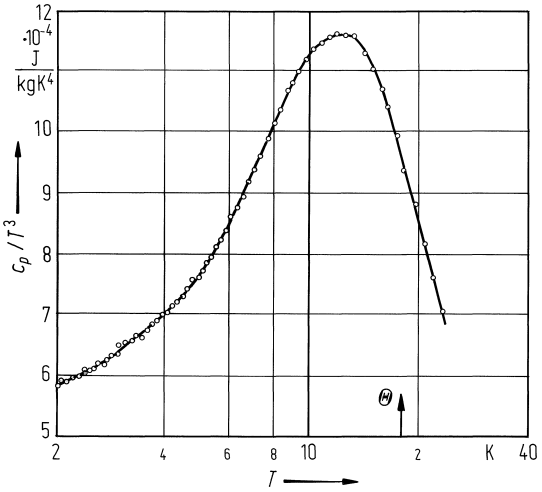

Fig. 1C-a16-012. $K(Ta_{0.988}Nb_{0.012})O_3$. c_p / T^3 vs. T [81Law].

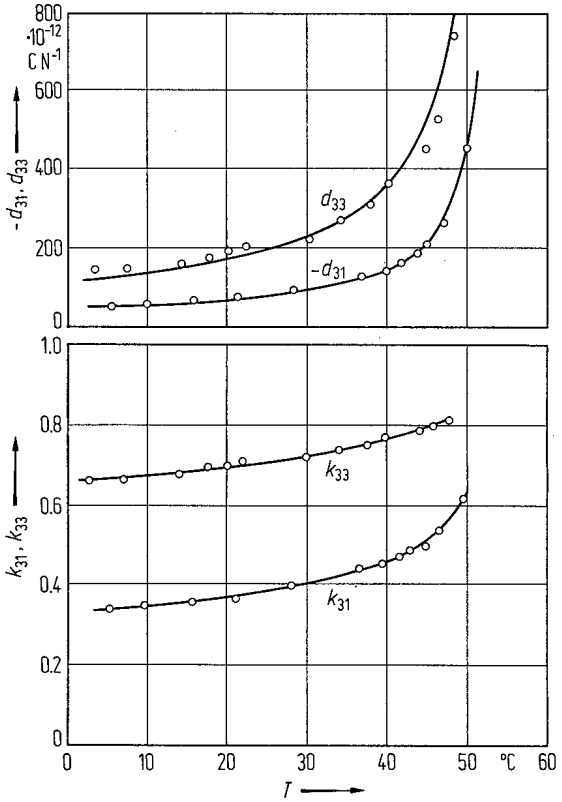

Fig. 1C-a16-013. $K(Ta_{0.55}Nb_{0.45})O_3$ (KTN). – d_{31}, d_{33}, k_{31}, k_{33} vs. T [72Ada].

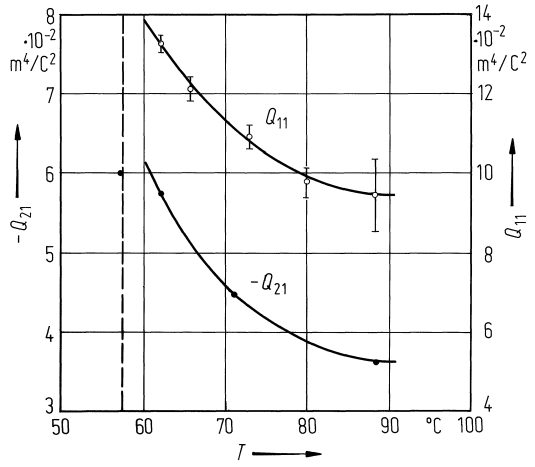

Fig. 1C-a16-014. $K(Ta_{0.55}Nb_{0.45})O_3$. Q_{11}, $-Q_{21}$ vs. T [82Uch]. $Q_{\lambda 1}$: electrostrictive constant ($S_\lambda = Q_{\lambda 1} P_1^2$).

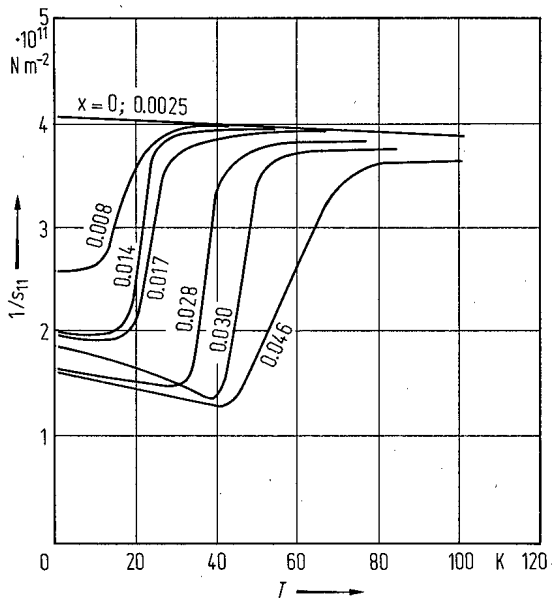

Fig. 1C-a16-015. $K(Ta_{1-x}Nb_x)O_3$. $1/s_{11}$ vs. T [77Hoc]. Parameter: x. s_{11}: elastic compliance.

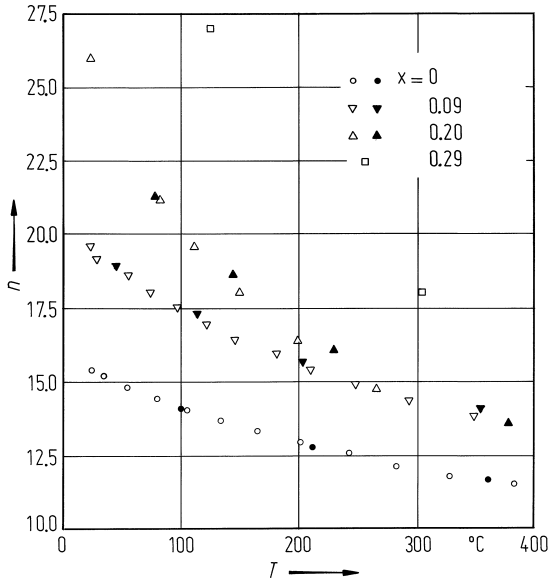

Fig. 1C-a16-016. $K(Ta_{1-x}Nb_x)O_3$. n vs. T [85Ryt]. Parameter: x. n: refractive index at 94 GHz.

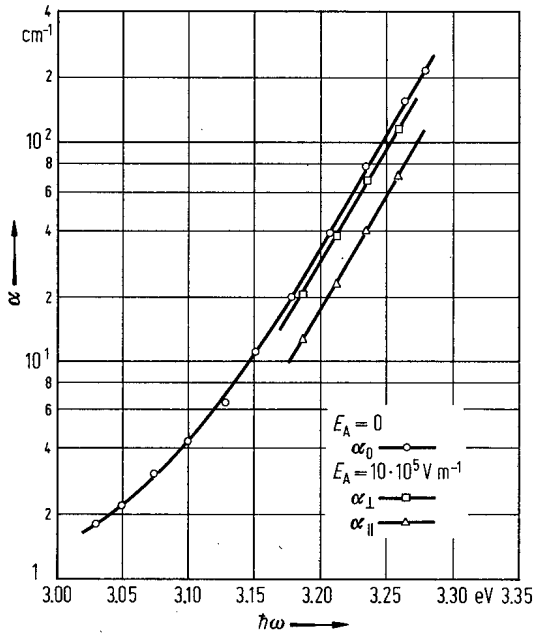

Fig. 1C-a16-017. $K(Ta_{1-x}Nb_x)O_3$ ($x \approx 0.34$). α vs. $\hbar\omega$ [72Man2]. Parameter: E_A (applied field). α: absorption coefficient at 23 °C, $\hbar\omega$: photon energy.

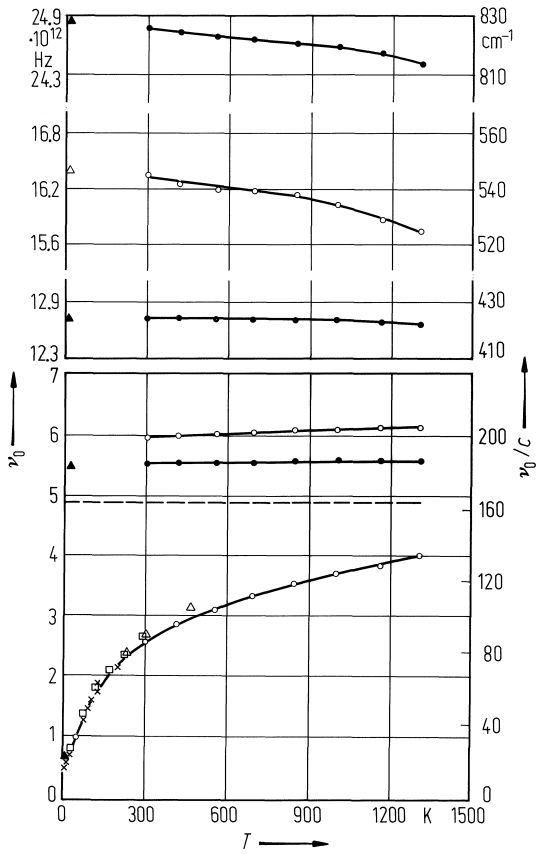

Fig. 1C-a16-018. $K(Ta_{0.982}Nb_{0.018})O_3$. ν_o vs. T [83Ryt]. ν_o: optical mode frequency obtained from infrared reflection spectra. Open and closed circles are TO and LO modes, respectively. For other symbols see original paper.

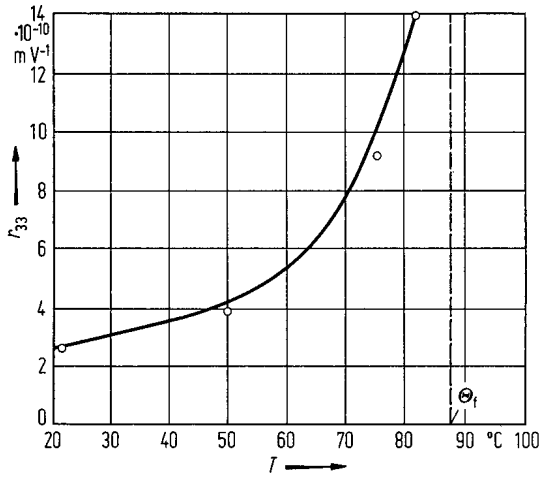

Fig. 1C-a16-019. $K(Ta_{0.52}Nb_{0.48})O_3$. r_{33} vs. T [67Haa]. λ = 546 nm.

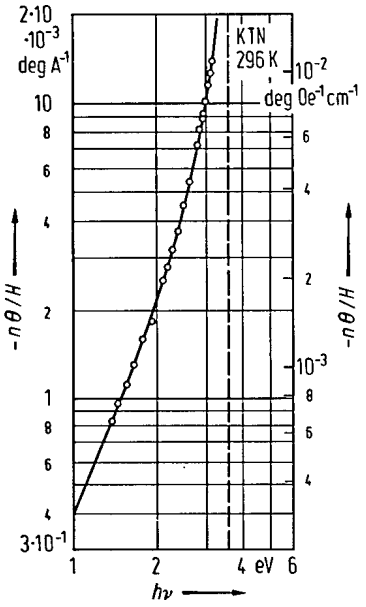

Fig. 1C-a16-020. KTN. – $n\theta$ / H vs. $h\nu$ [67Bae]. n: refractive index, θ: Faraday rotation per unit length, H: magnetic field intensity, $h\nu$: photon energy. Vertical dashed line indicates band gap energy (3.54 eV). 1 Oe = 79.58 A m^{-1}.

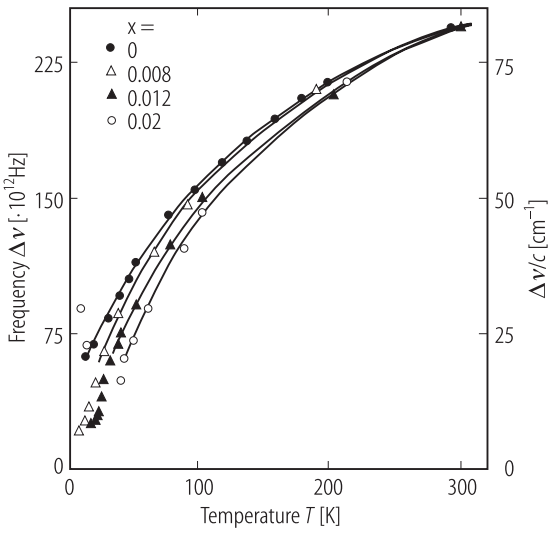

Fig. 1C-a16-021. $K(Ta_{1-x}Nb_x)O_3$. $\Delta\nu$ vs. T [88Kug]. Parameter: x. $\Delta\nu$: soft mode frequency obtained from hyper Raman scattering.

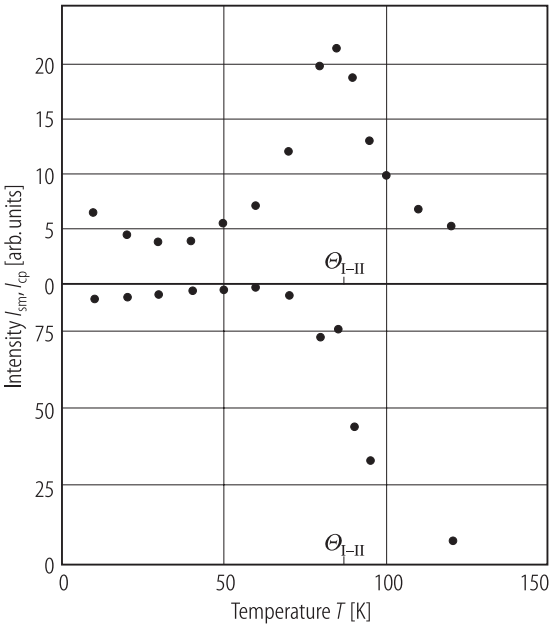

Fig. 1C-a16-022. $K(Ta_{0.91}Nb_{0.09})O_3$. I_{sm}, I_{cp} vs. T [90Fon]. I_{sm}: integrated intensity of the soft mode, I_{cp}: integrated intensity of the central peak of Raman scattering spectra in $z(xx)y$ geometry.

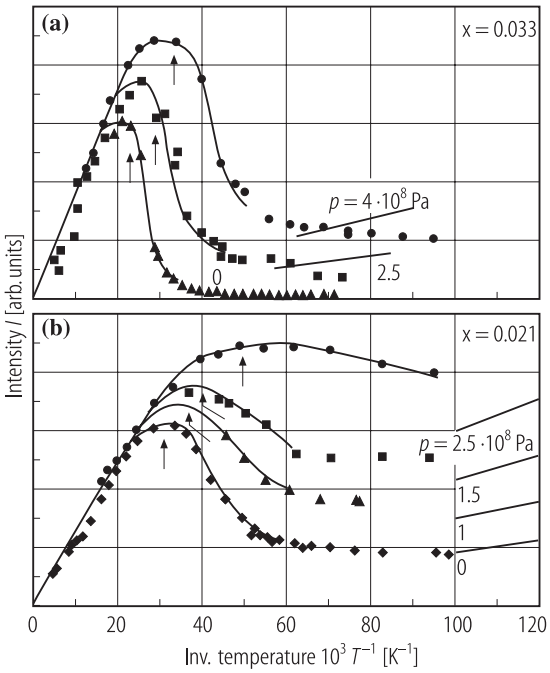

Fig. 1C-a16-023. $K(Ta_{1-x}Nb_x)O_3$. *I* vs. 1/*T* [94Rod]. (**a**) x = 0.033, (**b**) x = 0.021. Parameter: *p* . *I*: NMR signal for ^{181}Ta in arbitrary scale. Straight lines indicate the respective asymptotes toward low temperature. Arrows indicate the expected transition temperatures.

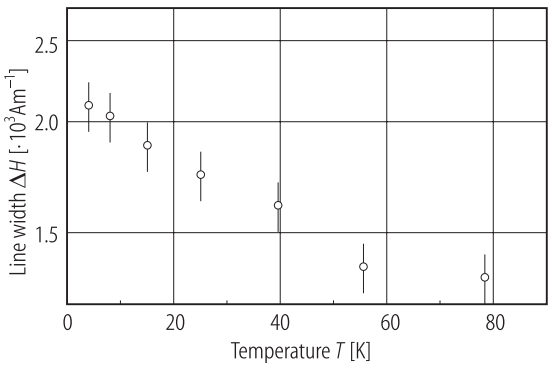

Fig. 1C-a16-024. $K(Ta_{0.94}Nb_{0.06})O_3$. ΔH vs. T [89Vug]. ΔH: line width of Fe^{3+} ESR for $\theta = 60^o$.

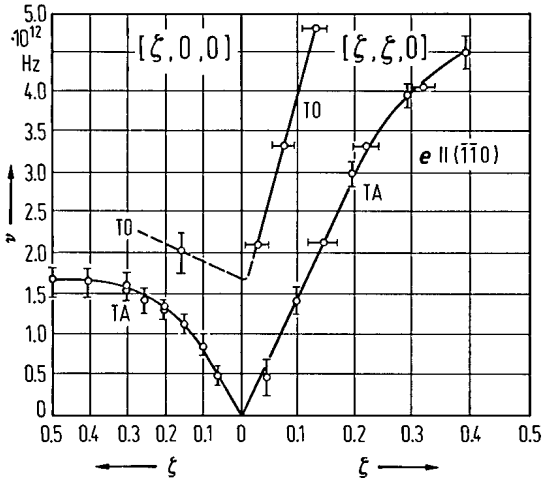

Fig. 1C-a16-025. $K(Ta_{0.63}Nb_{0.37})O_3$. Phonon dispersion curves [71Yel]. T = 65 °C.

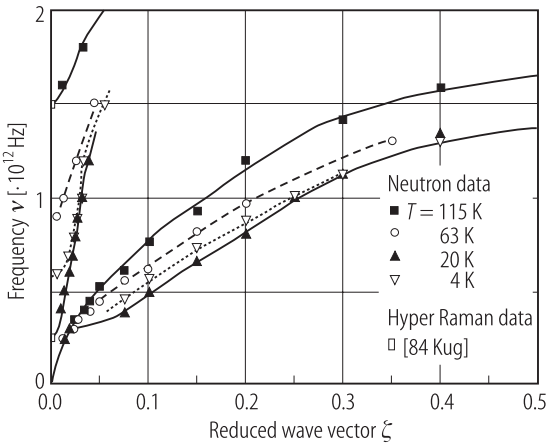

Fig. 1C-a16-026. $K(Ta_{0.988}Nb_{0.012})O_3$. ν vs. ζ [96Fou]. Parameter: *T*. Phonon dispersion measured by neutron scattering [96Fou] and hyper Raman scattering [84Kug]. ν: phonon frequency, ζ: reduced wave vector coordinate in [001] direction.

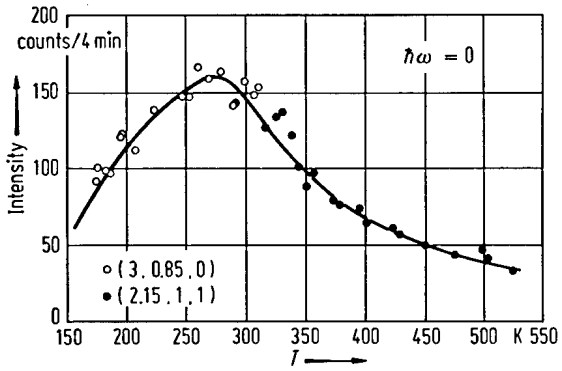

Fig. 1C-a16-027. $K(Ta_{0.56}Nb_{0.44})O_3$. *I* vs. *T* [71Yel]. *I*: soft mode intensity.

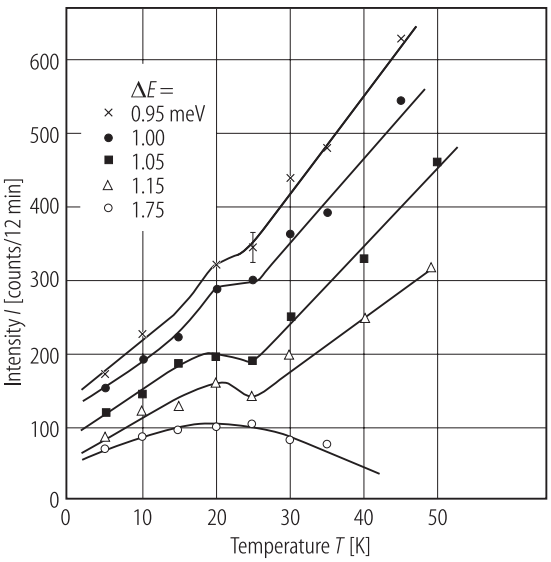

Fig. 1C-a16-028. $K(Ta_{0.988}Nb_{0.012})O_3$. *I* vs. *T* [90Cho]. Parameter: Δ*E*. *I*: neutron scattering intensity for constant –*Q* scan. ***Q*** = (0, 2, 0), E_i = 8.44 meV. Peaks at 20 K are indicative of mode-softening.

References

55Rei Reisman, A., Triebwasser, S., Holtzberg, F.: J. Am. Chem. Soc. **77** (1955) 4228.
59Hal Hall, J.H., Triebwasser, S.: J. Am. Chem. Soc. **81** (1959) 6394.
59Tri Triebwasser, S.: Phys. Rev. **114** (1959) 63.
66Bar Barker Jr., A.S.: Phys. Rev. **145** (1966) 391.
67Bae Baer, W.S.: J. Phys. Chem. Solids **28** (1967) 677.
67Fro Frova, A., Boddy, P.J.: Phys. Rev. **153** (1967) 606.
67Haa Haas, W., Johannes, R.: Appl. Opt. **6** (1967) 2007.
68Fle Fleury, P.A., Worlock, J.M.: Phys. Rev. **174** (1968) 613.
70Tod Todd Jr., L.T.: Master Thesis, Electrical Engineering Dept. MIT, 1970.
71Fox Fox, A.J., Whipps, P.W.: Electron. Lett. **7** (1971) 139.
71Yel Yelon, W.B., Cochran, W., Shirane, C., Linz, A.: Ferroelectrics **2** (1971) 261.
72Ada Adachi, M., Kawabata, A.: Jpn. J. Appl. Phys. **11** (1972) 1855.
72Hew Hewat, A.W., Rouse, K.D., Zaccai, G.: Ferroelectrics **4** (1972) 153.
72Man1 Manlief, S.K., Fan, H.Y.: Phys. Rev. B **5** (1972) 4046.
72Man2 Manlief, S.K., Fan, H.Y.: Phys. Rev. B **6** (1972) 185.
76Per Perry, C.H., Hayes, R.R., Tornberg, N.E.: Proc. Int. Conf. Light Scattering Solids, 3rd, held in Campinas, Brazil (1975), Balkanski, M., Leite, R.C.C., Porto, S.P.S. (eds.), Paris: Flammarion Sciences, 1976, p. 812.
77Boa Boatner, L.A., Höchli, U.T., Weibel, H.: Helv. Phys. Acta **50** (1977) 620.
77Hoc Höchli, U.T., Weibel, H.E.: Phys. Rev. Lett. **39** (1977) 1158.
80Boa Boatner, L.A., Krätzig, E., Orlowski, R.: Ferroelectrics **27** (1980) 247.
81Law Lawless, W.N., Rytz, D., Höchli, U.T.: Ferroelectrics **38** (1981) 809.
82Uch Uchino, K., Nomura, S., Cross, L.E.: J. Phys. Soc. Jpn. **51** (1982) 3242.
83Ryt Rytz, D., Fontana, M.D., Servoin, J.L., Gervais, F.: Phys. Rev. B **28** (1983) 6041.
84Kug Kugel, G., Vogt, H., Kress, W., Rytz, D.: Phys. Rev. B **30** (1984) 985.
84Sam Samara, G.A.: Phys. Rev. Lett. **53** (1984) 298.
85Lee Lee, E., Chase, L.L., Boatner, L.A.: Phys. Rev. B **31** (1985) 1438.
85Ryt Rytz, D., Klein, M.B., Bobbs, B., Matloubian, M., Fetterman, H.: Jpn. J. Appl. Phys. **24**, Suppl. 24-2 (1985) 1010.
86Tsu Tsukioka, M., Nagata, E., Ehara, S., Tanaka, J.: Jpn. J. Appl. Phys. **25** (1986) 918.
88Kug Kugel, G.E., Mesli, H., Fontana, M.D., Rytz, D.: Phys. Rev. B **37** (1988) 5619.
89Bal Baller, F., Gather, B., Hellermann, R., Hesse, H., Krätzig, E.: Phys. Status Solidi (a) **116** (1989) K195.
90Cho Chou, H., Shapiro, S.M., Lyons, K.B., Kjems, J., Rytz, D.: Phys. Rev. B **41** (1990) 7231.
90Fon Fontana, M.D., Bouziane, E., Kugel, G.E.: J. Phys. Condens. Matter **2** (1990) 8681.
90Tou Toulouse, J., Wang, X.M.: Ferroelectrics **106** (1990) 255.
91Som Sommer, D., Friese, D., Kleemann, W., Rytz, D.: Ferroelectrics **124** (1991) 231.
92Gut Gutmann, R., Hulliger, J., Wüest, H.: Ferroelectrics **134** (1992) 291.
92Wan Wang, M., Wang, J.Y., Liu, Y.G., Guan, Q.C., Wei, J.Q.: Ferroelectrics **132** (1992) 49.
93Fon Fontana, M.D., Maglione, M., Höchli, U.T.: J. Phys. Condens. Matter **5** (1993) 1895.
93XuH Xu, H.P., Li, Q., Feng, D., Shen, G.J., Guan, Q.C., Wang, J.Y.: Ferroelectrics **146** (1993) 137.
94Ger Gerhard-Multhaupt, R., Yilmaz, S., Bauer, S., Ren, W.: Ferroelectrics **157** (1994) 359.
96Fou Foussadier, L., Fontana, M.D., Kress, W.: J. Phys. Condens. Matter **8** (1996) 1135.